Dimensionless analysis of the unstart boundary for 2D mixed hypersonic inlets

J. Chang , D. Yu , W. Bao and L. Qu
Harbin Institute of Technology
China

ABSTRACT

Inlet unstart boundary is one of the most important issues of the hypersonic inlet and is also the foundation of the protection control of a scramjet. To solve this problem, the 2D internal steady flow of a 2D mixed internal/external compression hypersonic inlet was numerically simulated at different freestream conditions and backpressures with a RANS (Reynolds-Averaged Navier-Stokes) solver using a RNG (Renormalisation Group) k-ε turbulence model, and two different inlet unstart phenomena were analysed. The dimensional analysis method was introduced to find the essence variables describing the inlet unstart boundary based on "numerical experimental" data in this paper. The dimensionless pressure ratios of the forebody and isolator were analysed respectively. The results show that the unstart boundary of the 2D mixed hypersonic inlet is determined by M_0, α and Re_0. Pressure ratio π increases with M_0 increasing, and it increases firstly and decreases then with α increasing. Pressure ratio π increases with Re_0 increasing. Re_0 ($Re_0 < 2 \times 10^7$) has a major effect on π and Re_0 ($Re_0 > 2\times10^7$) has little effect on π.

NOMENCLATURE

r	ratio of specific heats
k	turbulent kinetic energy
l_i	the length of the wedge
M_0	freestream Mach number
M_1	mass-weighed averaged Mach number at the entrance of the isolator
M_2	Mach number at the cross section 2-2' shown in Fig.1
M_{s0}	starting Mach number at the cross section 0-0' shown in Fig.1
M_{s2}	starting Mach number at the cross section 2-2' shown in Fig.1
p_0	freestream static pressure
p_1	mass-weighed averaged static pressure at the entrance of the isolator
p_2	maximum mass-weighed averaged static pressure at the exit of the isolator
p_b	mass-weighed averaged static pressure at the exit of the isolator
p_d	dynamics pressures of the vehicle
p_s	surface pressure of the hypersonic inlet
Re_0	unit Reynolds number of the freestream
Re_1	unit Reynolds number at the entrance of the isolator
u_0	velocity of the freestream
u_1	velocity at the entrance of the isolator
x	axis location of the hypersonic inlet
y	vertical location of the hypersonic inlet
α	angle-of-attack of the freestream
β_i	shock angle
ρ_0	density of the freestream
ρ_1	density at the entrance of the isolator
μ	viscosity of the freestream
π	p_2/p_0, maximum pressure ratio of the inlet

Paper No. 3267. Manuscript received 19 December 2007, revised version received 31 December 2007, accepted 13 May 2008.

https://doi.org/10.1017/S0001924000002505 Published online by Cambridge University Press

π_1 p_1/p_0, pressure ratio of the forebody
π_2 p_2/p_1, maximum mass-weighed averaged pressure ratio of the isolator
δ_i the angle of the wedge
ε turbulent dissipation rate

1.0 INTRODUCTION

The unstart phenomenon is one of the most important issues of the hypersonic inlet. The disturbances which can induce inlet unstart can be either the variation of flight conditions (i.e. angle-of-attack, freestream Mach number, freestream pressure, etc.) or the disturbance from the combustor. For hypersonic airbreathing engines, inlet unstart causes a large drop of both engine thrust and specific impulse, thus it may cause catastrophic damage during hypersonic flight[1,2]. Unstart phenomena must be controllable to insure the safety and success of the mission. Because the maximum performance of the inlet is at the boundary between start and unstart, it is difficult to compensate for the poor off-design performance. There have been various means proposed for unstart prevention, such as changing geometry structure, bleeding, regulating fuel supply and so on. But these solutions focus on reducing the inlet performance; it is undesirable since the performance of the inlet is a critical factor to the hypersonic air breathing engine. In order to maintain high performances without crossing the unstart boundary, an active unstart margin predictor and controller is necessary. The goal of the inlet protection control system is to determine the unstart boundary, predict inlet unstart before it occurs, take some measures to mitigate the inlet unstart or to initiate inlet restart. The first step need to do for the inlet protection control is the analysis and expression of unstart boundary of hypersonic inlets, and it is the research emphasis of this paper.

Unstart phenomena of the hypersonic inlet have been very active fields of research for some three decades, there have been many investigations devoted to this subject[3-14]. Generally speaking, there are two approaches to the inlet unstart. The first one is based on numerical simulation. With current powerful computers, Computation Fluid Dynamics (CFD) can be used as a preliminary tool to analyze the phenomena and mechanism of the inlet unstart. Mayer and Paynter[3,4] used an Euler solver and simulated an axisymmetric inlet unstart due to the variation of freestream variables such as temperature, velocity and pressure. Neaves and McRae[5] developed dynamic solution-adaptive gird algorithm introduced by Benson and McRae[6] and simulated the 3D inlet unstart caused by a combustor perturbation. Zha[7,8] investigated unstart transient mechanism of a typical axisymmetric HSCT (High Speed Civil Transport) inlet at angle-of-attack using CFD. Cox[9] presented several mechanisms of hypersonic inlet unstart, including backpressure unstart, overcontraction unstart and turning angle unstart. Yu[10] anlaysed two different inlet unstart phenomena and investigated the classification criterions of hypersonic inlet start/unstart. The second approach is based on experimental investigation. Schmitz[11] and Van Wie[12] analysed the major factors that influence the inlet operation mode and studied the start/unstart characteristic of a 2D hypersonic inlet. Reinartz[13] and Saied Emami[14] studied the variation of the isolator geometry and its influence on the overall inlet compression efficiency, the investigation shows that the sustainable backpressure is strongly influenced by the isolator length. Cox[9] discussed the concepts for preventing unstart and approaches for unstart margin control, but how to analyse and express the unstart boundary is not given in detail.

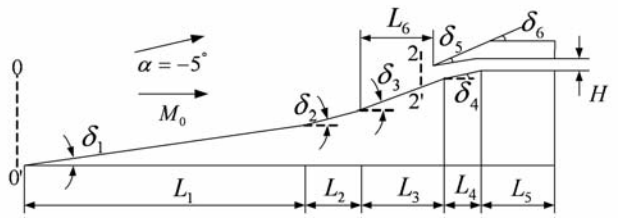

Figure 1. Geometric sketch of the inlet model.

Table 1
Geometric parameters of the hypersonic inlet

L_1/m	L_2/m	L_3/m	L_4/m	L_5/m	L_6/m
0·267	0·068	0·085	0·035	0·095	0·074
δ_1/°	δ_2/°	δ_3/°	δ_4/°	δ_5/°	δ_6/°
10	15	20	14	10·2	24

The first step in modeling any physical phenomena is the identification of the relevant variables, then relating these variables via known physical laws. For sufficiently simple phenomena, we can usually construct a quantitative relationship among these variables based on physical laws. However, for many complex phenomena which often occur in engineering applications, the modeling is often difficult, if not impossible. In these situations, modeling methods are indispensable, and one of the most powerful modeling methods is dimensional analysis. The basic idea is that physical laws do not depend on arbitrariness in the choice of the basic units of measurement. For the modeling of the unstart boundary of a hypersonic inlet, the relationship between the unstart boundary and the freestream conditions can not be denoted in an analytical expression due to its complexity. So it is necessary to introduce the tool of dimensional analysis to find the essence factors describing the unstart boundary based on the 'numerical simulation or experimental data'. The benefit of dimensional analysis is that, reduce the dimension of influence factors of the unstart boundary, and reduce the complexity and cost of the research.

In this paper, the 2D internal steady flow of a hypersonic inlet was numerically simulated in different freestream conditions and backpressures with a RANS solver using a RNG k-ε turbulence model. Based on the numerical simulation data, the dimensionless pressure ratios of forebody and isolator were analysed respectively utilising the tool of dimensional analysis, then the major factors that influence the inlet unstart boundary are discussed.

2.0 INLET MODEL AND NUMERICAL METHOD

2.1 Inlet model

The overall inlet geometry is based on the similar inlet model tested within the frame of earlier CIAM/NASA flight test[15]. The computational model includes an inlet and constant area isolator only. Figure 1. shows the geometric sketch of inlet model. The main geometric parameters of the hypersonic inlet are referred to Table 1.

2.2 Numerical method

The computation is performed using the Finite-Volume technique with upwind discretisation to solve the two-dimensional compressible Reynolds-Averaged Navier-Stokes equations. The air is considered to be a calorically perfect gas with constant ratio of specific heat, $\gamma = 1{\cdot}4$. The space discretisation is performed by a cell-centered formulation. To account for the directed propagation of information in the inviscid part of the equations, the advection upstream splitting method (AUSM) flux vector splitting is applied

https://doi.org/10.1017/S0001924000002505 Published online by Cambridge University Press

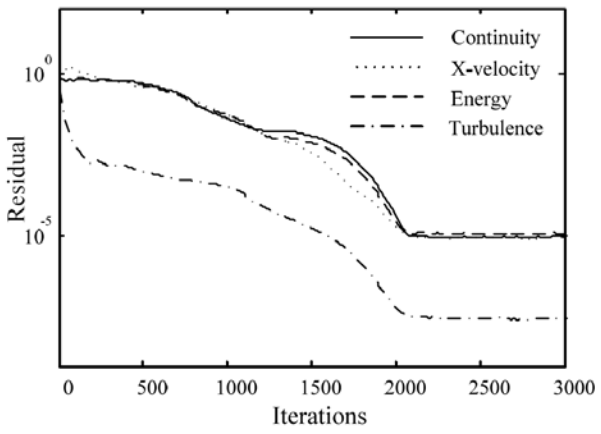

Figure 2. Residuals for the hypersonic inlet computation.

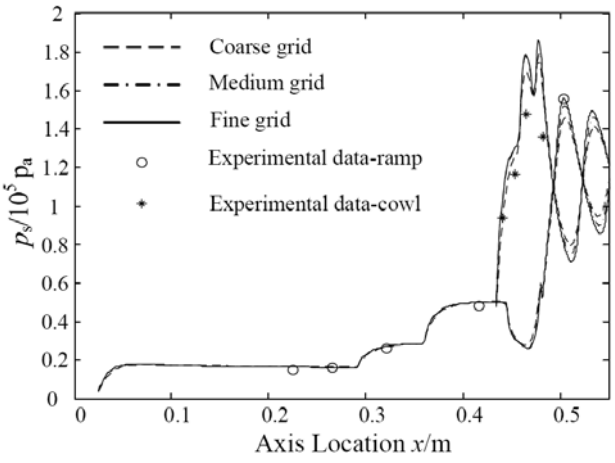

Figure 3. Surface pressure distributions for refined grids, $M_0 = 6{\cdot}4$, $T_0 = 203{\cdot}5$K, $p_0 = 3968$Pa.

for the approximation of the convective flux functions. Higher-order accuracy for the upwind discretisation and consistency with the central differences used for the diffusive term is achieved by the monotonic upstream scheme for conservation laws extrapolations, and the total variation diminishing property of the scheme is ensured by the Van Leer flux limiter. Time integration is performed by an explicit five stage Runge–Kutta time-stepping scheme. To enhance convergence, a multigrid method, implicit residuals smoothing, and local time stepping are applied.

A renormalisation group k-ε turbulence model is implemented for turbulent flows. The near-wall treatment adopts non-equilibrium wall functions which are recommended for use in complex flows involving separation, reattachment, and impingement where the mean flow and turbulence are subjected to severe pressure gradients and change rapidly. The supersonic inflow is defined by specifying the boundary conditions, where the definition of α is referred to Fig.1. In case of predominant supersonic outflow, the variables are completely extrapolated from the interior to the boundary. Otherwise, the influence of the throttle is simulated with a prescribed backpressure p_b at the outflow boundary and the remaining variables are extrapolated. At solid walls, the no-slip boundary condition is enforced by setting the velocity components to zero. The adiabatic energy boundary condition is directly applied by zeroing the contributions of the wall faces to the dissipative fluxes.

2.3 Numerical accuracy analysis

To ensure convergence of the numerical solution, the residuals (L_2-norm) are monitored in Fig. 2. The solution can be considered as converged after approximately 3,000 iterations. At this stage, the continuity residual, x-velocity residual, and energy residual reach their minimum values after falling for over four orders of magnitude. The turbulence residual has a six orders of magnitude decrease. An additional convergence criterion enforced in this current analysis requires the difference between computed inflow and outflow mass flux to drop below 0·5%. The evaluation was performed using the coarse mesh.

The performance of a grid sensitivity analysis confirms that the grid resolution used here is sufficient to capture the physically relevant features. To ensure the accuracy of the turbulence flow solution, a value of y^+ below five is realised for the main portion of the wall flow region. To simulate the interaction between the shock and the boundary layer, the intersection and reflection of wave system, calculate the flow field at first, and perform the technology of mesh self-adaptation based on the pressure gradient and continue to compute. In Fig. 3, the static pressure distributions along the cowl and the ramp surfaces are shown for three different grid-refinement levels: coarse (754 × 65), medium (1,020 × 110), and fine (1,810 × 205); the maximum discrepancy between the three mesh levels is less than 5%. The calculations were performed on a workstation. The CPU time needed for computation is about 1h for the coarse mesh, 3·5h for the medium mesh, and 9h for the fine mesh. Out of this analysis, the medium grid was selected, and all results shown are computed applying this resolution. The use of a medium grid resolution saves the CPU time greatly.

The accuracy of the current numerical investigation is evaluated by comparison with the experimental results. The experimental data is referred to Fig. 4 (a, b) in Ref[15]. The surface pressure distributions are shown in Fig. 3, allow for a qualitative comparison between numerical and experimental results, where the freestream conditions are $M_0 = 6{\cdot}4$, $T_0 = 203{\cdot}5$K, $p_0 = 3968$Pa. Here, a discrepancy in the surface pressure distributions can be seen, but the both overall pressure distributions are consistent.

2.4 Analysis of inlet unstart phenomena

The inlet unstart probably occurs at the range Mach 3 to Mach 12, it is most likely at the low Mach number. The risk to the vehicle increases as velocity increases. The inlet unstart at higher Mach number might be too much overpressure for the inlet structure to handle without larger vehicle weight penalties. At low Mach number, the vehicle might be catastrophically uncontrollable after inlet unstart, even if the structure could handle inlet unstart overpressures. There are two main different classes of inlet unstart for the fixed geometry hypersonic inlet, one is backpressure unstart, and the other is low Mach number unstart.

Firstly, we discuss the backpressure unstart of hypersonic inlets. In scramjet, a precombustion shock system is developed inside of the isolator because of the subsequent high-pressure combustion zone. To produce a similar shock wave system in the test, the effect of the operating engine is simulated by a specified backpressure. The surface pressure distributions with different backpressure are shown in Fig 4. The high backpressure leads to the separation of the boundary layer. The pressure buildup proceeds continuously due to the rapidly growing boundary layer. As the backpressure increases, the onset of pressure buildup moves upstream into the isolator. At $p_b/p_0 = 33{\cdot}5$, the complete isolator contributes to the pressure buildup and the maximum pressure ratio p_b/p_0 is achieved. After even a slight shift of the operating point ($p_b/p_0 = 33{\cdot}5$), the pressure rise is pushed forward into the contracting part of the inlet. A further increase of the backpressure causes a severe flow blockage and results in a strong decrease of captured mass flow. In this condition, the inlet

https://doi.org/10.1017/S0001924000002505 Published online by Cambridge University Press

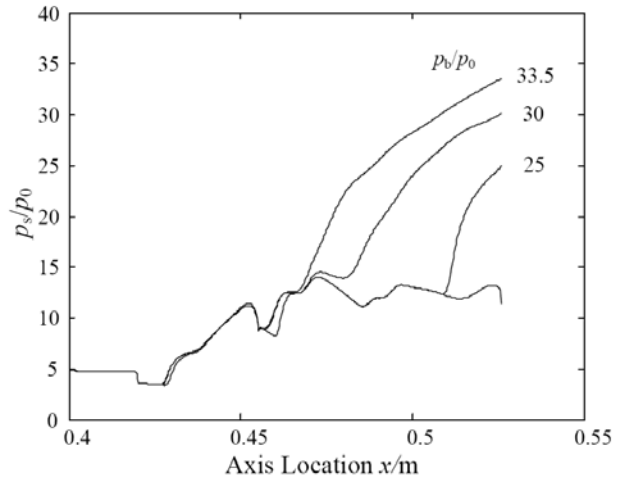

Figure 4. Surface pressure distributions with different backpressures of the hypersonic inlet in this paper, $M_0 = 4$ and $\alpha = 0$.

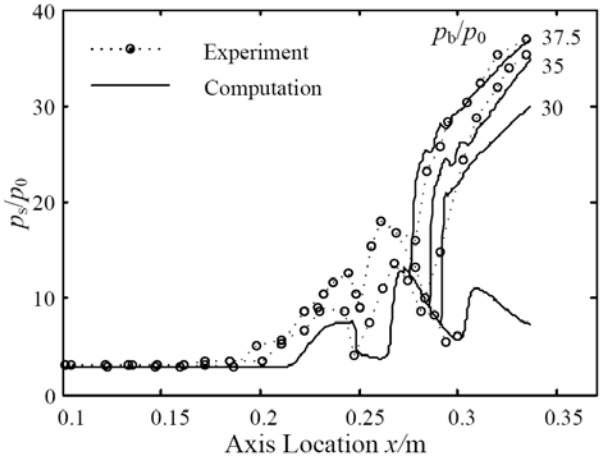

Figure 5. Surface pressure distributions with different backpressures of the hypersonic inlet in Ref (14), $M_0 = 4$ and $\alpha = 0$.

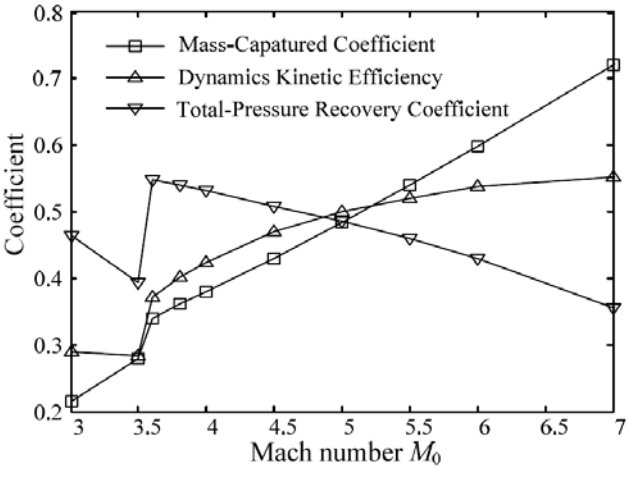

Figure 6. Variations of the performance index with M_0.

flowfield is unstable and the inlet is no longer started. The accuracy of the current numerical method on the backpressure unstart is evaluated by comparison with the experimental results. The inlet model and experimental data are referred to Fig. 7 and Fig. 19(e) in Ref. (14). The surface pressure distributions with different backpressures are shown in Fig. 5, allow for a qualitative comparison between numerical and experimental results. Here, a discrepancy in the ramp pressure distributions can be seen, but the both overall pressure distributions are consistent and the maximal pressure ratios before inlet unstart are both 37·5. The maximal pressure ratios is the backpressure unstart boundary value of hypersonic inlets at $M_0 = 4$ and $\alpha = 0$, and it proves that the backpressure unstart boundary of hypersonic inlets can be obtained exactly by the CFD code in this paper. The reason for the discrepancy is probably the deficiency of the turbulence model, the differences between experiment and computation conditions or the measurements error of sensors.

Then we analyse the low Mach number unstart of hypersonic inlets. The internal area contraction ratio of the hypersonic inlet is about 1·7, which is above the Kantrowitz limit for self starting. Figure 6 shows the variations of mass-capture ratio, total-pressure recovery and kinetic energy efficiency with freestream Mach number, where the performance index is referred to the one (mass-averaged) at the exit of the isolator. The Mach number contours of hypersonic inlets at different M_0 are shown in Fig. 7. As freestream Mach number decreases, the mass-capture and kinetic energy efficiency gradually decrease and the total-pressure recovery increases. When Mach number decreases to 3·5, the performance parameter varies abruptly because the separated flow appears and the backward shock is formed, thus the inlet is no longer started and it belongs to the low Mach number unstart phenomena. This class of unstart phenomenon is low Mach number unstart. The starting Mach number M_{s0} is 3·5 at the attack-of-angle zero, and it can be validated by flight test[15]. So the CFD code used in this paper can exactly predict the starting Mach number of hypersonic inlets.

In a word, the computation results of the hypersonic inlet accord with the physical conception of the aerodynamics, and the numerical accuracy analysis of this CFD code has been validated by Ref[10,16]. It can reveal the intersection of oblique shock waves and expansion waves and capture the primary characteristic of internal flowfield, and can exactly predict the backpressure unstart boundary and low Mach number unstart boundary of hypersonic inlets.

3.0 DIMENSIONLESS ANALYSIS OF THE UNSTART BOUNDARY FOR HYPERSONIC INLETS

Generally speaking, for the fixed-geometry hypersonic inlet, the operation modes depends on the freestream pressure, the freestream temperature, the freestream velocity, the freestream viscosity, the angle-of-attack and the backpressure of the isolator. The backpressure unstart is formed due to the larger backpressure or the lower pressure of freestream. The low Mach number unstart occurs when freestream Mach number is less than the starting Mach number, which results in a larger separated region appearing that facilitates the backward shock and the inlet unstart. The unstart boundary of the hypersonic inlet includes the boundary of backpressure unstart and the boundary of low Mach number unstart. The boundary of backpressure unstart is referred to the maximum pressure ratio of inlet π at different freestream conditions, where π is the critical pressure ratio above which the backpressure unstart will occur. The boundary of low Mach number unstart is referred to M_0 at different α, where M_0 is the critical Mach number under which the low Mach number unstart will occur.

https://doi.org/10.1017/S0001924000002505 Published online by Cambridge University Press

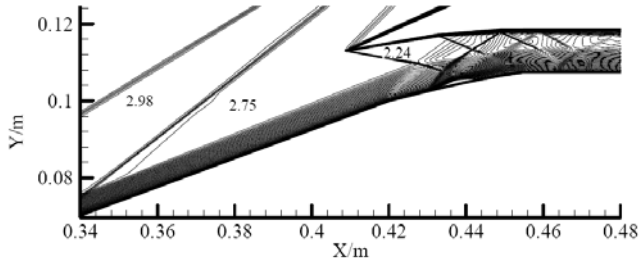

a) $M_0 = 4$.

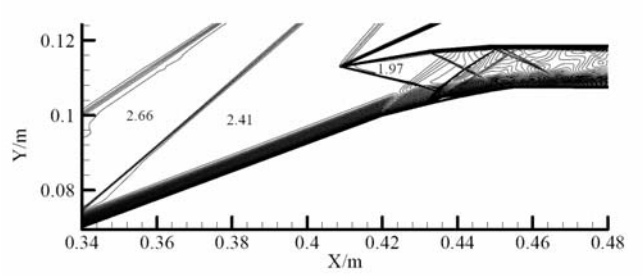

b) $M_0 = 3{\cdot}6$.

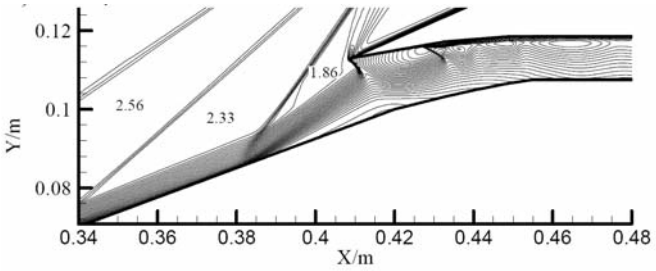

c) $M_0 = 3{\cdot}5$.

Figure 7. Mach number contour of hypersonic inlets at different M_0

3.1 Dimensionless analysis of π_1

The freestream is compressed by several oblique shock generated by the external compression surface, which is referred to Fig. 8. The magnitude of p_1 depends on the conditions of freestream (static pressure p_0, velocity u_0, density ρ_0, viscosity μ and angle-of-attack α), the type of inlet, the length of wedge l_i, the angle δ_i. There exists a mapping relation between them:

$$p_1 = f(p_0, u_0, \rho_0, \alpha, \mu, l_i, \delta_i) \quad \ldots(1)$$

Where *f* means that there exists a function, and it does not denote the detailed expression.

There exist eight variables and three dimensions for system (1). Define l_i, u_0 and ρ_0 as the basic variable of this problem, utilise $\prod$ theorem[17] based on the dimensional analysis, and the dimensionless function can be obtained as:

$$p_1/(\rho_0 u_0^2) = f(p_0/(\rho_0 u_0^2), \alpha, \mu/(\rho_0 u_0 l_1), l_i/l_1, \delta_i) \quad \ldots(2)$$

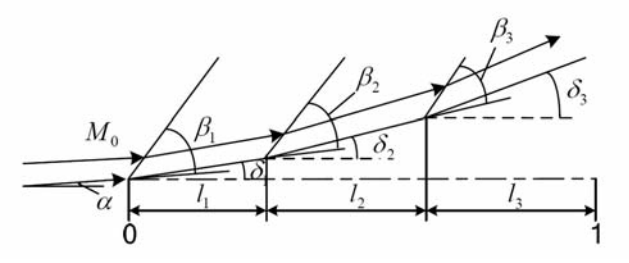

Figure 8. The sketch of the forebody.

The Equation (2) can be transformed to

$$\pi_1/(rM_0^2) = f(1/(rM_0^2), \alpha, \mathrm{Re}_0, l_i/l_1, \delta_i) \quad \ldots(3)$$

The flow similar conditions of two forebodies are: 1) The geometry is similar, l_i/l_1 and δ_i are constant. 2) The adiabatic index *r* is constant. 3) M_0 and Re_0 are constant. For a fixed geometry hypersonic inlet, l_i/l_1 and δ_i are constant; the flow medium is air, *r* is constant. Equation (3) can be rewritten as in this case

$$\pi_1 = f(M_0, \alpha, \mathrm{Re}_0) \quad \ldots(4)$$

For a fixed hypersonic inlet, the Equation (1) can be transformed to

$$p_1 = f(p_0, u_0, \rho_0, \alpha, \mu) \quad \ldots(5)$$

There exist four and six variables for system (4) and (5) respectively. Suppose ten operation points are used for each variable, the number of the total numerical simulations or experiments of the hypersonic inlet is 10^4 and 10^6 respectively. The number decreases 100 times by introducing the tool of dimensional analysis, and it can reduce greatly the complexity and cost of the research.

Equation (4) means that π_1 depends on M_0, α and Re_0. These influence factors are analysed respectively below. Firstly Re_0 is fixed, the effect of M_0 and α on π_1 is discussed. In this case, the Equation (4) can be rewritten as :

$$\pi_1 = f(M_0, \alpha) \quad \ldots(6)$$

Figure 9. shows the variation of pressure ratio π_1 with α at different M_0. With α increasing, the angle of the several oblique shock is added and the pressure ratio π_1 increases when M_0 is fixed. With M_0 increasing, Mach number in the front of the several oblique shock is added and the pressure ratio π1 increases when α is fixed.

The starting Mach number M_{s0} and M_{s2} are about 3·5 and 2·4 at the attack-of-angle zero. With α increasing, the angles of the several oblique shocks are added and M_2 decreases when M_0 is fixed. M_2 is less than 2·4 when α is more than 6 degrees at $M_0 = 4$, at this time the low Mach number unstart occurs. The unstart angles-of-attack at M_0 4, 5, 6 and 7 are 6, 11·25, 15 and 17 degrees respectively. The low Mach number unstart boundary of the hypersonic inlet which is shown in Fig. 9.

Secondly M_0 and α are fixed, Re_0 is altered by changing p_0. The effect of Re_0 on π_1 is discussed below and Equation (4) can be rewritten as in this case

$$\pi_1 = f(\mathrm{Re}_0) \quad \ldots(7)$$

https://doi.org/10.1017/S0001924000002505 Published online by Cambridge University Press

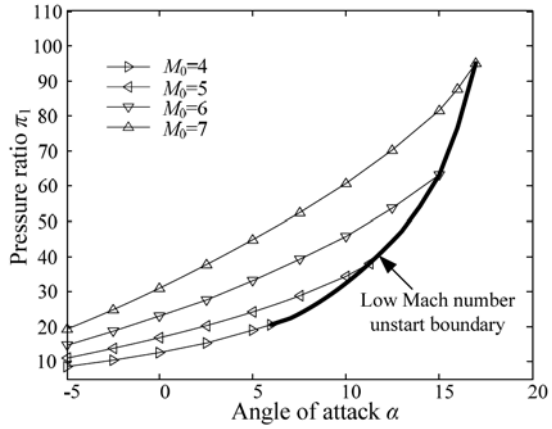

Figure 9. Effects of α on π_1

At hypersonic speeds the development of the boundary layer within an inlet has a major influence on the performance and operability of the inlet. This influence arises because the growth of the boundary-layer changes the effective compression of the captured flow. The boundary layer thickness will change with Re_0 varied, which results in the variation of the angle and strength of oblique shocks.

The velocity vectors of the hypersonic inlet at different Reynolds numbers are shown in Fig.10. The larger Re_0 is, the thinner is the boundary-layer thickness, the smaller are the angle of the oblique shocks. These effects would necessarily result in the variation of π_1. Figure 11. shows the variation of π_1 with Re_0 at different α. With Re0 increasing, the pressure ratio π_1 is a little decrease when α is fixed. Re_0 ($Re_0 < 2 \times 10^7$) has a major effect on π_1 and Re_0 ($Re > 2 \times 10^7$) has little effect on π_1.

As discussed above, π_1 is related to M_0, α and Re_0 for the fixed geometry hypersonic inlet. That is:

$$\pi_1 = f(M_0, \alpha, Re_0) \quad \ldots (8)$$

In the same way, M_1 and Re_1 are related to M_0, α and Re_0. That is:

$$M_1 = f(M_0, \alpha, Re_0) \quad \ldots (9)$$

$$Re_1 = f(M_0, \alpha, Re_0) \quad \ldots (10)$$

Figures 12 and 13 show the variation of M_1 with α at different M_0 and the variation of M_1 with Re_0 at different α respectively. The strength of the oblique shock increased with α increasing, which results in the decrease of M_1. The strength of the oblique shock decreased with Re_0 increasing, which results in the increase of M_1. Re_0 ($Re_0 < 2 \times 10^7$) has a major effect on M_1 and Re_0 ($Re_0 > 2 \times 10^7$) has little effect on M_1. Figure 14 and Fig. 15 show the variation of Re_1 with α at different M_0 and the variation of Re_1 with Re_0 at different α respectively. Re_1 increases firstly and then decreases with α, and increases with Re_0.

3.2 Dimensionless analysis of π_2

The isolator plays an important role on scramjet, it reduces the perturbation of inlet and combustor, maintains the continuous

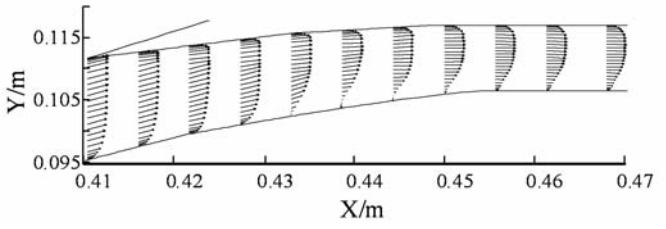

a) Velocity vectors of the inlet at $Re_0 = 0{\cdot}20 \times 10^7$

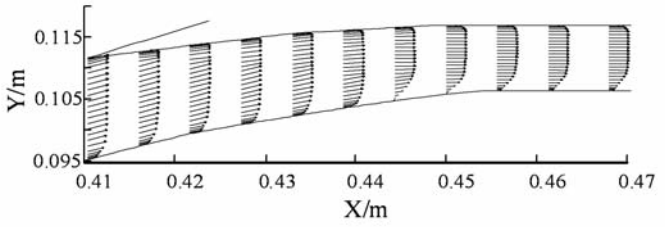

b) Velocity vectors of the inlet at $Re_0 = 1{\cdot}01 \times 10^7$

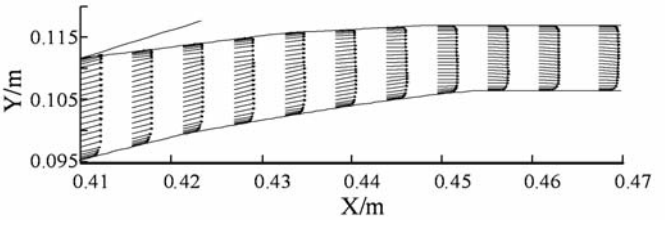

c) Velocity vectors of the inlet at $Re_0 = 6{\cdot}07 \times 10^7$.

Figure 10. Velocity vectors of the hypersonic inlet at different Re_0.

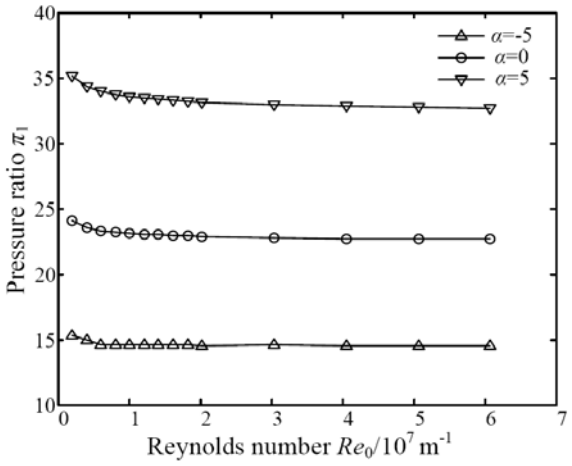

Figure 11. Effects of Re_0 on π_1.

operation conditions, guarantees that the engine works in wider range of Mach number. The isolator is assumed below: its length is l, its height is d, the flow medium is air, which is shown in Fig. 16. The magnitude of p_2 depends on static pressure p_1, velocity u_1, density ρ_1, viscosity μ, the length l and the height d, where p_2 is the maximum pressure at the exit of isolator. There exists a mapping relation between them:

$$p_2 = g(p_1, u_1, \rho_1, d, l, \mu) \quad \ldots (11)$$

https://doi.org/10.1017/S0001924000002505 Published online by Cambridge University Press

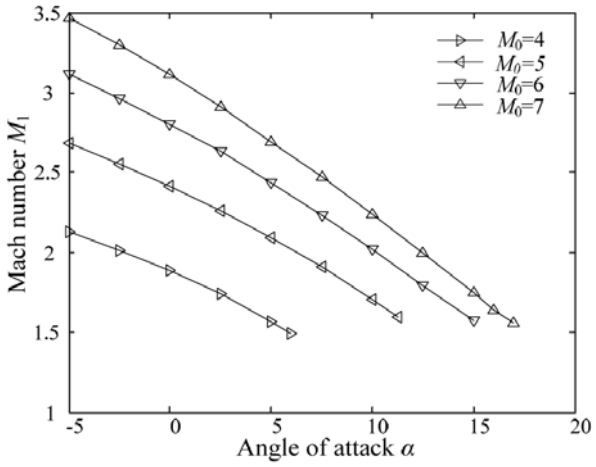

Figure 12. Effects of α on M_1.

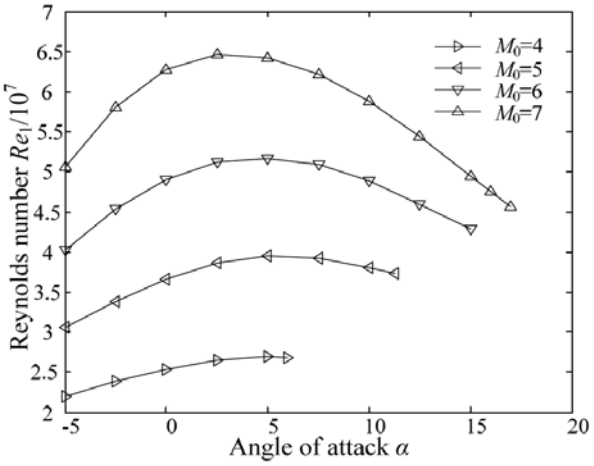

Figure 14. Effects of α on Re_1.

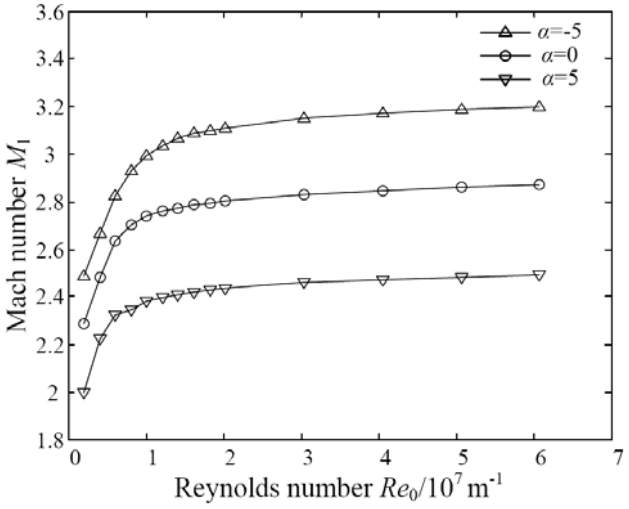

Figure 13. Effects of Re_0 on M_1.

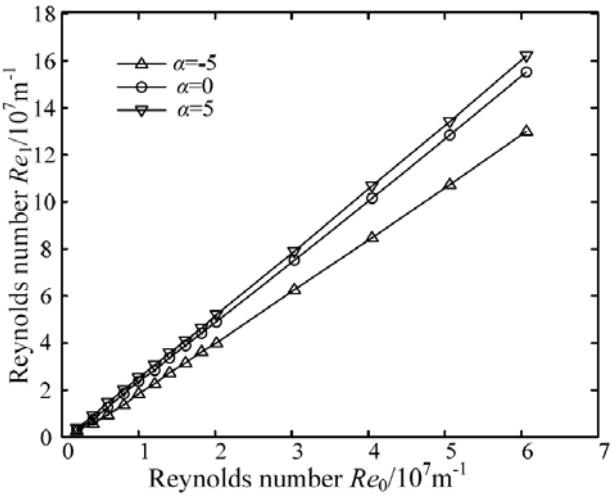

Figure 15. Effects of Re_0 on Re_1.

Where *g* denotes that there exists a function relation, and it does not denote the detailed expression.

There exist seven variables and three dimensions for system (11). Define u_1, ρ_1 and d as the basic variable of this problem, utilise theorem based on the dimensional analysis, and the dimensionless function can be obtained as:

$$p_2/(\rho_1 u_1^2) = g(p_1/(\rho_1 u_1^2), l/d, \mu/\rho_1 u_1 d) \quad \ldots (12)$$

The Equation (12) can be transformed to

$$\pi_2 /(rM_1^2) = g(1/(rM_1^2), l/d, \mathrm{Re}_1) \quad \ldots (13)$$

The flow similar conditions of two isolators are: 1) The geometry is similar, *l/d* is constant. 2) The adiabatic index *r* is constant. 3) M_1 and Re_1 are constant. For a fixed geometry isolator, *l/d* is constant; the flow medium is air, *r* is constant. Equation (13) can be rewritten as in this case

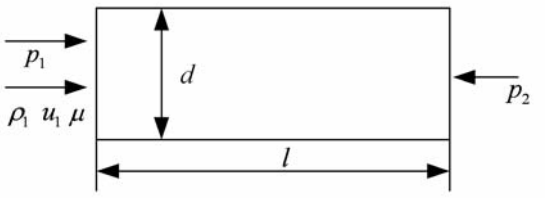

Figure 16. The sketch of the isolator.

$$\pi_2 = g(M_1, \mathrm{Re}_1) \quad \ldots (14)$$

It means that π_2 depends on M_1 and Re_1. These influence factors are analyzed respectively below. When the isolator is sustained by the maximum static pressure p_2, the high backpressure leads to the separation of the boundary layer and the pressure buildup proceeds continuously due to the rapidly growing boundary layer. A further increase of the backpressure ($p_b > p_2$) causes a severe flow blockage

https://doi.org/10.1017/S0001924000002505 Published online by Cambridge University Press

and results in a strong decrease of captured mass flow. The inlet flowfield is unstable and the inlet is no longer started in this case, where the unstart is used to denote the operation condition under which the shock system structures in the internal portions of the inlet alter the mass-captured characteristics. The underlying mechanism for separation is that the cumulative upstream viscous forces have removed the momentum necessary for the boundary layer flow to overcome the imposed pressure rise. The larger M_1 and Re_1 are, the larger π_2 is. Combined with (9) and (10), the following equation can be obtained.

$$\pi_2 = g(M_0, \alpha, \mathrm{Re}_0) \quad \ldots (15)$$

It means that π_2 depends on M_0, α and Re_0. These influence factors are analysed respectively below. Firstly Re_0 is fixed, the effect of M0 and α on π_2 is discussed. Equation (15) can be rewritten as in this case.

$$\pi_2 = g(M_0, \alpha) \quad \ldots (16)$$

Figure 17 shows the variation of pressure ratio π_2 with α at different M_0. With α increasing, π_2 decreases when M_0 is fixed. With M_0 increasing, π_2 increases when α is fixed.

Secondly M_0 and α are fixed, Re_0 is altered by changing p_0. The effect of Re_0 on π_2 is discussed below and Equation (15) can be rewritten as in this case.

$$\pi_2 = g(\mathrm{Re}_0) \quad \ldots (17)$$

Figure 18 shows the variation of π_2 with Re_0. With Re_0 increasing, π_2 increases. Re_0 ($Re_0 < 2 \times 10^7$) has a major effect on π_2 and Re_0 ($Re_0 > 2 \times 10^7$) has little effect on π_2. Comparing Figs 17 and 18 with Fig. 12 and Fig. 13, we can find that the variation of π_2 with α and Re_0 is similar to the variation of M_1 with α and Re_0 respectively. It can be concluded that Ms_1 plays a main role on π_2 in contrast with Re_1.

4.0 DIMENSIONLESS ANALYSIS OF UNSTART BOUNDARY

The unstart boundary of the hypersonic inlet includes the boundary of the backpressure unstart and the boundary of the low Mach number unstart. The boundary of the backpressure unstart is referred to the maximum pressure ratio of inlet π at different freestream conditions, where π is the critical pressure ratio above which the backpressure unstart will occur. Pressure ratio π can be obtained by fitting the data. The boundary of the low Mach number unstart is referred to M_0 at different α, where M_0 is the critical Mach number under which the low Mach number unstart will occur. As can be seen from above, the pressure ratio at the boundary of backpressure unstart $\pi = \pi_1 \times \pi_2 = f(M_0, \alpha, Re_0) \times g(M_0, \alpha, Re_0) = F(M_0, \alpha, Re_0)$, namely the backpressure unstart boundary of the hypersonic inlet can be obtained by M_0, α and Re_0.

Figure 19. shows that the variation of π with α at different M_0 respectively. With M_0 increasing, Mach number in the front of the several oblique shock is added and the pressure ratio π increases when α is fixed. With α increasing, the angles of the several oblique shocks are added and π increases firstly when M_0 is fixed. M_2 decreases with α increasing when M_0 is fixed, which results in π falls at higher α. When M_2 is less than the M_{s2}, the low Mach number unstart phenomena occurs. The low Mach number unstart boundary

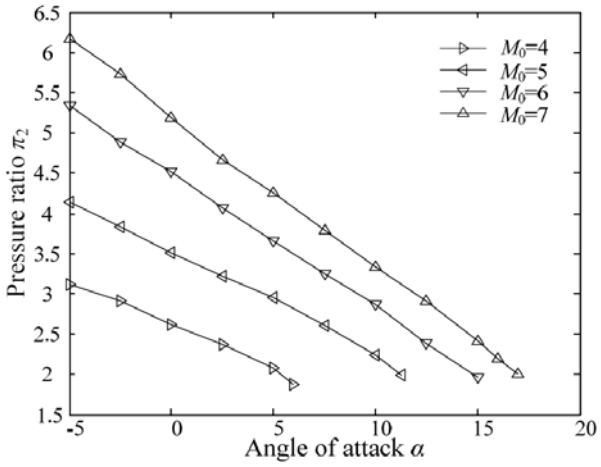

Figure 17. Effects of α on π_2.

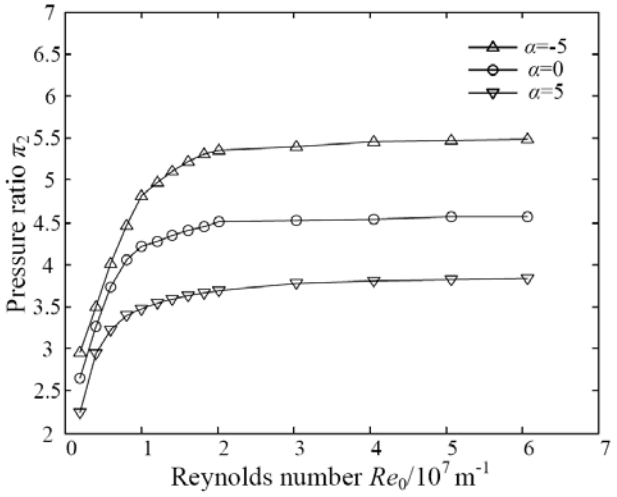

Figure. 18 Effects of Re_0 on π_2.

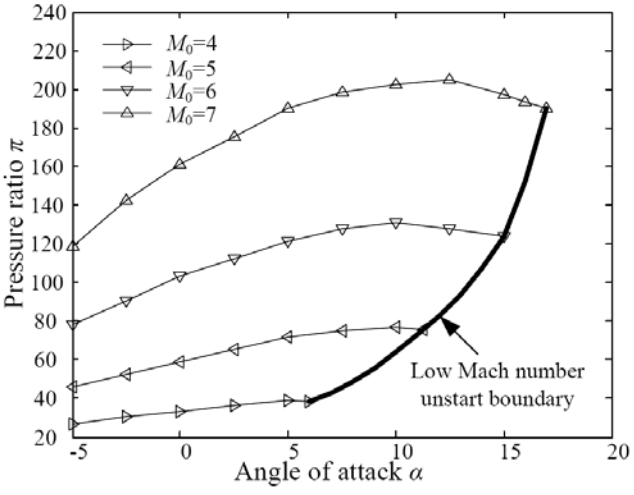

Figure 19. Effects of α on π.

https://doi.org/10.1017/S0001924000002505 Published online by Cambridge University Press

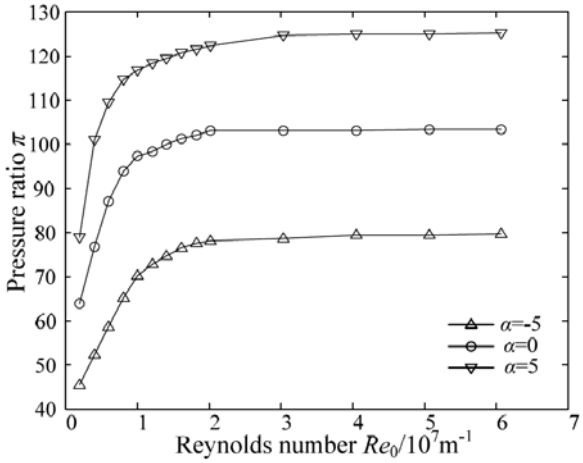

Figure 20. Effects of Re_0 on π.

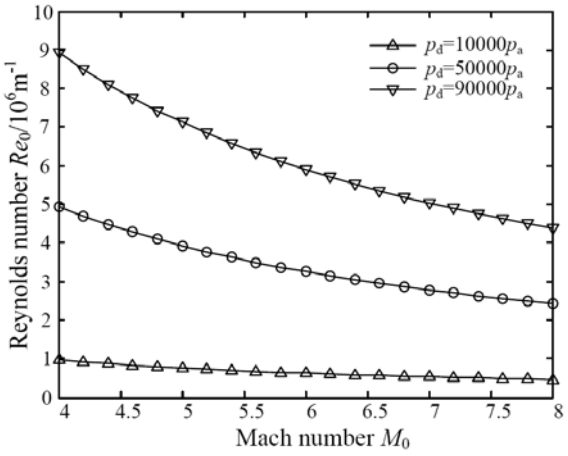

Figure 21. Effects of M_0 on Re_0.

of the hypersonic inlet is shown in Fig.19. Figure 20 shows that the variation of π with Re_0 at different α. With Re_0 increasing, π increases. Re_0 ($Re_0 < 2 \times 10^7$) has a major effect on π and Re_0 ($Re_0 > 2 \times 10^7$) has little effect on π.

The freestream conditions are mainly determined by the flight envelope which can be denoted by the dynamic pressure q_0. For a hypersonic vehicle, if q_0 is too large, the structural forces and the drag on the vehicle can be excessive. On the other hand, if q_0 is too small, the wing area required for sustained flight may become unreasonably large. This explains hypersonic vehicles may end up being designed to operate within a fairly narrow range[18] of q_0, approximately 20,000-90,000N/m^2. The variation of the unit Reynolds number Re_0 with M_0 at different dynamic pressures is shown in Fig. 21, and the range of Re_0 is belong to $0{\cdot}45 \times 10^6$ and 9×10^6. Comparing Fig. 21 with Fig. 20, we can conclude that Re_0 has a main effect on the pressure ratio characteristic of the inlet at the flight envelope. So the effects of Re_0 on the boundary of the backpressure unstart need to be considered.

5.0 CONCLUSIONS

The dimensionless analysis of the unstart boundary for 2D mixed compression hypersonic inlets is investigated. For this investigation, the tool of dimensional analysis is introduced to find the essence variables describing the unstart boundary in this paper. The results show that the unstart boundary of the hypersonic inlet is determined by M_0, α and Re_0. Pressure ratio π increases with M_0 increasing when α is fixed. Pressure ratio π firstly increases and then decreases with α increasing when M_0 is fixed. Pressure ratio π increases with Re_0 increasing when α is fixed. Re_0 ($Re_0 < 2 \times 10^7$) has a major effect on π and Re_0 ($Re_0 > 2 \times 10^7$) has little effect on π.

REFERENCE

1. CAMPBELL, D.H. F-12 series aircraft propulsion system performance and development, *J of Aircr*, **11,** (11), 1974, pp 670–676.
2. SEDDON, J. and GOLDSMITH, E.L. *Intake Aerodynamics,* AIAA Educational Series, AIAA, Washington DC, 1989, pp 149–168.
3. MAYER, D. and PAYNTER, G.C. Prediction of supersonic inlet unstart caused by freestream disturbances, *AIAA J,* **33,** (2), 1995, pp 266-275.
4. MAYER, D. and PAYNTER, G.C. Boundary conditions for unsteady supersonic inlet analyses, *AIAA J,* **32,** (6), 1994, pp 1200-1206.
5. NEAVES, M.D., MCRAE, D.S. and EDWARDS, J.R. High-speed inlet unstart calculations using an implicit solution adaptive mesh algorithm, AIAA Paper 2001-0825, January 2001.
6. BENSON, R.A. and MCRAE, D.S, Numerical simulations of the unstart phenomenon in supersonic inlet/diffuser, AIAA Paper 1993-2239, June 1993.
7. ZHA, G.C., KNIGHT, D. and SMITH D. Numerical investigations of high speed civil transport inlet unstart transient at angle of attack, *AIAA J of Aircr*, **35,** (6), 1998, pp 851-856.
8. ZHA, G.C., KNIGHT, D. and SMITH D. Numerical simulation of high speed civil transport inlet operability with angle of attack, *AIAA J of Aircr*, **36,** (7), 1998, pp 1223-1229.
9. COX, C., LEWIS, C. and PAP. R. Prediction of unstart phenomena in hypersonic aircraft, AIAA Paper 1995-6018, April 1995.
10. YU, D., CHANG, J., BAO, W. and XIE, Z. Optimal classifications criterions of hypersonic inlet start/unstart, *J of Propul and Power*, **23,** (2), 2007, pp 310-316.
11. SCHMITZ, D.M. and BISSINGER, N.C. Design and testing of fixed-geometry hypersonic intakes, AIAA Paper 1998-1529, April 1998.
12. VAN WIE, D.M. and KWOK, F.T. Starting characteristics of supersonic inlets, AIAA Paper 1996-2914, July 1996.
13. REINARTZ, B.U. and HERRMANN, C.D. Aerodynamic performance analysis of a hypersonic inlet isolator using computation and experiment, *J of Propul and Power*, **19,** (5), 2003, pp 868-875.
14. EMAMI, S. and TREXLER, C.A. Experimental investigation of inlet-combustor isolators for a dual-mode scramjet at a Mach number of 4, NASA Technical Paper 3502, May 1995.
15. Rodriguez, C.G. Computational fluid dynamics analysis of the central institute of aviation motors/NASA scramjet, *J of Propul and Power*, **19,** (4), 2003, pp 547-555.
16. CUI, T., YU, D., CHANG, J. and BAO, W. Topological geometry interpretation of hypersonic inlet start/unstart-catastrophe, hysteresis and bifurcation, *AIAA J of Aircr*, **45**, (4), 2008, pp 1464-1468.
17. BARENBLATT, G.I., *Dimensional Analysis,* Gordon and Breach Science Publishers, New York, 1987.
18. HEISER, W.H. and PRATT. D.T. *Hypersonic airbreathing propulsion,* AIAA Educational Series, AIAA, Washington DC, 1994, pp 37-39.

https://doi.org/10.1017/S0001924000002505 Published online by Cambridge University Press